BIBECHANA
Vol. 21, No. 3, December 2024, 311-320

ISSN 2091-0762 (Print), 2382-5340 (Online)
Journal homepage: http://nepjol.info/index.php/BIBECHANA
Publisher: Dept. of Phys., Mahendra Morang A. M. Campus (Tribhuvan University) Biratnagar

Experimental FTIR characterization of kidney stones, DFT analysis of CaC_2O_4 and its interactions with lysozyme

Arjun Acharya[1], Madan Khanal[1], Rajesh Maharjan[1], Kalpana Gyawali[1], Kamal Khanal[1], Mohan Bahadur Kshetri[1], Bhoj Raj Luitel[2], Rameshwar Adhikari[3,4], Deependra Das Mulmi[5], Tika Ram Lamichhane[1,*], Hari Prasad Lamichhane[1],

[1]*Central Department of Physics, Tribhuvan University, Kathmandu 44600, Nepal*
[2]*Department of Urology and Kidney Transplant Surgery, Tribhuvan University , Teaching Hospital, Institute of Medicine, Maharajgung, Kathmandu 44600,Nepal*
[3]*Central Department of Chemistry, Tribhuvan University, Kathmandu 44600, Nepal*
[4]*Research Center for Applied Science and Technology (RECAST), Tribhuvan University, Kathmandu 44600, Nepal*
[5]*Nanomaterials Research Laboratory, Nepal Academy of Science and Technology, Lalitpur 44700, Nepal*

[*]Corresponding author: Email: tika.lamichhane@cdp.tu.edu.np

Abstract

Kidney stone is an alarming global disease due to its rising incidence and prevalence. FTIR spectroscopic analysis reveals that calcium oxalate is one of the most frequent chemical constituents in kidney stones. DFT calculations indicate that the calcium oxalate can interact through charge transfer process in biological activities. Among various proteins, lysozyme is one of the promoter proteins in nephrolithiasis of calcium oxalate type kidney stone. The location, conformation and interactions of calcium oxalate with the active residues of lysozyme contribute the binding energy of -4.18 kcal/mol. The characterization of kidney stones, DFT calculations of calcium oxalate, and binding interactions of calcium oxalate-lysozyme complex contribute to the understanding of nephrolithiasis.

Keywords
Kidney stone; Calcium oxalate; Lysozyme; Fourier transform infrared spectroscopy; Density functional theory; Molecular docking; Nephrolithiasis.

Article information
Manuscript received: August 14, 2024; Revised: September 25, 2024; Accepted: September 26, 2024
DOI https://doi.org/10.3126/bibechana.v21i3.68781

1 Introduction

Kidney stone is one of the oldest diseases, characterized by the formation of solid masses within the urinary system. These deposits are strongly linked to chronic kidney disease and can lead to kidney failure [1, 2]. Despite increased awareness and improved treatment procedures, the prevalence of kidney stone disease is increasing globally, presenting a significant health threat [3]. The prevalence ranges from 7% to 13% in North America, 5% to 9% in Europe, and 1% to 5% in Asian countries [4]. In Asia, the western, southern, and southwestern regions exhibit particularly high rates, with prevalence ranging from 5% to 19.1%. In contrast, East Asian and Northern Asian regions show a lower prevalence, ranging from 1% to 8% [5].

The study in Kathmandu University Teaching Hospital about the distribution of urinary calculi based on age, gender and types shows 54.20% cases are of 21-40 years. Among the total kidney stone patients, male population (57.95%) are more prone than the female population (42.05%). Again, 74.16% of the total patients are suffered from calcium oxalate and calcium phosphate type urinary calculi. Non-vegetarian groups (88.70%) are found more suffered from this disease than vegetarian groups (11.30%). Further, this study also suggested spectroscopic analysis of urinary calculi [6]. Computed tomography (CT) urographic study in Lumbini Medical College, Palpa, Nepal shows 76.7% of urinary obstruction are due to urinary calculi. Among the patients, 60.7% are male and 39.3% are female, and 46.7% of patients lie within 21-40 years [7]. In another research of urinary calculi in Kathmandu Pathology Laboratory using biochemical techniques shows calcium oxalate as a major constituents with male to female patients ratio 1: 1.2 [8]. In a study of urinary calculi patients in Shree Birendra Hospital, Kathmandu, Nepal, it is found that 69.2 % of the affected population are male and 30.8% are female. The majority of patients, 51%, fall within the age range of 31-45 years. Additionally, calcium oxalate is found in 64.25% of the cases. Among the ethnic groups, maximum number (30.75%) of the patients are from the Janajati community, while minimum (11.25%) are from the Madhesi population. Geographically, 85.7% of the cases are reported in the Hilly region, with 14.3% originating from the Terai/Madhesh region [9].

Kidney stones are generally developed from calcium oxalate, calcium phosphate, magnesium ammonium phosphate, uric acid, and cystine. Among all, calcium oxalate (CaC_2O_4) is the most frequently observed in the kidney stones [10]. Fourier transform infrared (FTIR) spectroscopic technique is a powerful analytical tool for the prediction of chemicals in the samples through the measurement of wide range of spectra. It has high sensitivity, quantitative accuracy, and superior signal-to-noise ratio [11] and is widely used in the characterization of different types of kidney stones [12, 13]. Density functional theory (DFT) analysis can be employed to study the dipole moment, frontier molecular orbitals, global reactive descriptors, molecular electrostatic potential (MEP), and Mulliken atomic charges. These quantum mechanical properties provide insights about the potential interactions between chemical compound and protein, as explained in our previous work [14, 15].

Different proteins contribute as promoter in the biomineralization. In kinetic studies of calcium oxalate type crystal growth in the presence of proteins lactoferrin and lysozyme revealed that both the proteins promote crystal growth, with lysozyme exhibiting a more effective role in accelerating the growth process [16]. In our previous work, lactoferrin protein has exhibited the binding efficacy of -3.86 kcal/mol [14] and this research focuses on studying the different interactions by active amino acids of lysozyme protein and their contribution for binding efficacy with calcium oxalate at the atomic level.

Molecular docking analysis of protein and ligand can predict the different conformation of ligand within the selected binding pocket of target protein. It also predicts the binding affinities using different algorithms and scoring function [17]. The molecular docking of ligand with matrix proteins of kidney stones is found to be significant for studying the calcium oxalate types nephrolithiasis [18]. Such studies at the atomic level will be helpful for understanding the interactions between calcium oxalate and lysozyme.

Current research aims to characterize the kidney stones. Further, this research will study the quantum mechanical properties of calcium oxalate using DFT in water solvent, along with the interactions within binding domain of promoter protein, lysozyme. This study will contribute to the understanding of globally challenged and unclear phenomena of nephrolithiasis.

2 Methodology

2.1 Characterization of samples

Kidney stones were collected from the institute of medicine, Maharajgung following the receipt of approval from the Institutional Review Committee of the Institute of Medicine, Tribhuvan University, Nepal. Informed consents were taken from all respondents for the analysis of samples. The collected stones were carefully cleaned with distilled water and air-dried at room temperature, then

crushed using mortar and pestle. Finally, samples were characterized under FTIR spectroscopy using the SHIMADZU IRAffinity-1S spectrophotometer within the range of 400-4000 cm^{-1}.

2.2 Quantum mechanical calculations

Three dimensional structure of calcium oxalate (ID: 33005) was obtained from PubChem, an open chemistry database at the National Institutes of Health, USA [19], and optimized using the DFT at B3LYP/6-311++G(d,p) level of calculation in the water solvent using the integral equation formulation of the polarizable continuum model (IEFPCM) in Gaussian 16W software [20]. Using the optimized structure, dipole moment, Mulliken charges, molecular electrostatic potential (MEP), highest occupied molecular orbital (HOMO) and lowest unoccupied molecular orbital (LUMO), and density of states (DOS) were calculated.

The energies of HOMO and LUMO orbitals, ionization potential and electron affinity of chemical compound were calculated using Koopmans' theorem as [21]:

$$\text{Ionization potential}, I = -E_{\text{HOMO}} \quad (1)$$

$$\text{Electron affinity}, A = -E_{\text{LUMO}} \quad (2)$$

The global reactive descriptors (chemical hardness, chemical softness, electronic chemical potential, and global electrophilicity index) were calculated using ionization potential and electron affinity as follows [21–23]:

$$\text{Chemical hardness: } \eta = \frac{I - A}{2} \quad (3)$$

$$\text{Chemical softness: } S = \frac{1}{\eta} \quad (4)$$

$$\text{Electronic chemical potential: } \mu = -\frac{I + A}{2} \quad (5)$$

$$\text{Global electrophilicity index: } \omega = \frac{\mu^2}{2\eta} \quad (6)$$

Additionally, ultraviolet-visible (UV-Vis) spectra were generated using the time-dependent (TD)-DFT method at the same level of calculation in water solvent. The compound was visualized and evaluated using GaussView 6 [24] and GaussSum 3.0 [25] software programs.

2.3 Molecular docking

The structure of human lysozyme (7xf6.pdb) was downloaded from the data center for the global protein data bank, RCSB PDB [26]. The secondary structures were analyzed by Ramachandran plot using Discovery Studio Visualizer v21.1.0.20298 [27]. The surface area, volume, and active residues in the binding region were predicted using the computed atlas of surface topography of the universe of proteins (CASTp) open-access online server [28]. The PDB files of protein and ligand were converted into partial charge and atom type (PDBQT) format after removal of water molecules, addition of Kollmann's charges, and integration of polar hydrogen atoms using the AutoDockTools [29–31]. Molecular docking using AutoDock4 [29] was carried out within the grid points (40× 40 × 40) of grid point spacing 0.375 Å along the x, y, and z axes, respectively. All the molecular docking procedures were conducted as described in our previous studies [14, 32]. Finally, the best conformation of protein-ligand complex was generated using the graphical user interface of AutoDockTools. The visualization of protein-ligand complexes were carried out using PyMOL 2.5.2 [33] and LigPlot+ v.2.2 [34].

3 Results and discussion

3.1 Experimental FTIR characterization of kidney stones

FTIR spectroscopic analysis was carried out for forty-four kidney stones. Comparing the generated spectra with literature [12,13], the samples contains whewellite, struvite, and uric acid types chemicals in pure and mixed form (Figure 1). The spectra of majority of the samples show intense peaks at 1608-1613 cm^{-1} and 1313-1315 cm^{-1} with less intense peak at 1380-1388 cm^{-1} (Figure 2) and these peaks almost match with the calcium oxalate monohydrate (whewellite) type kidney stones [12]. In our previous work, FTIR spectra of calcium oxalate generated in different solvent using DFT method at the B3LYP/6-311++G(d,p) level of calculation, the spectra in water solvent was closely matched with the experimental FTIR spectra of whewellite [14].

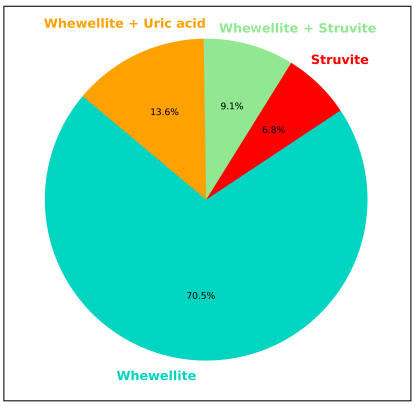

Figure 1: Pie chart showing the distribution of chemical compositions in the samples analyzed by Fourier transform infrared spectroscopic technique.

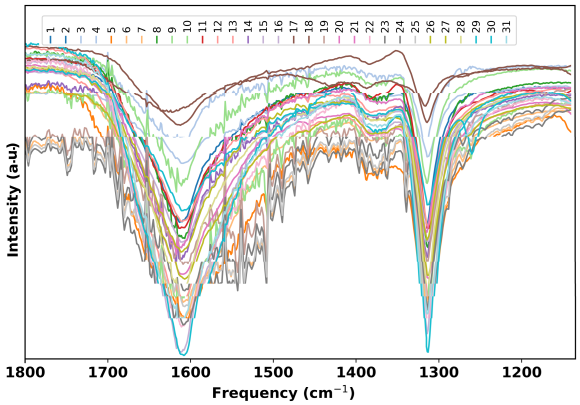

Figure 2: Experimental Fourier transform infrared spectra of the thirty-one whewellite type kidney stone samples.

3.2 Quantum mechanical calculation of calcium oxalate

3.2.1 Geometry optimization

The optimized structure of calcium oxalate is shown in Figure 3. In the present study, calculated dipole moment in water solvent is found 24.28 Debye, whereas in our previous work in gaseous phase, it was 14.88 Debye [14]. The dipole-dipole interactions between ligand and protein can affect the binding energy of the protein-ligand complex [35]. Thus, calcium oxalate can also interact through dipole-dipole interactions with the nephrolithiatic proteins.

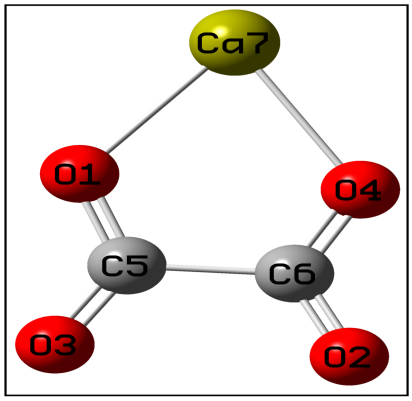

Figure 3: Optimized structures of CaC_2O_4 by the DFT method at the B3LYP/6-311++G(d,p) level of calculation in water solvent.

3.2.2 Frontier molecular orbitals

In the electronic absorption spectra of calcium oxalate in water solvent, the wavelengths of 278 nm, 265 nm, and 231 nm are responsible for the electronic transitions (Table 1). The maximum oscillatory strength is observed for wavelength 231 nm which is due to major contribution from the HOMO to LUMO+1 transition of electrons (Figure 4a and Table 1). The electronic absorption of calcium oxalate in water solvent shows close agreement with the experimental finding [36] compared to the results obtained in the gas phase [14]. The majority of charge density is concentrated around the carbon and oxygen atoms in HOMO, LUMO, and HOMO-1 orbitals. However, in LUMO+1, the charge density localized around calcium atom (Figure 4b). This visual representation reflects the charge distribution within the compound [37]. The energy gap, difference between the energies of HOMO and LUMO orbitals, is found to be 5.90 eV (Figure 4a). The number of states per unit energy interval at a given energy level in both occupied and virtual orbitals is illustrated with the DOS spectrum in Figure 5. The HOMO and LUMO orbitals and the spectra of DOS resemble closely each other. These results suggest that calcium oxalate can promote charge transfer process and exhibits enhanced capability for biological activities [38].

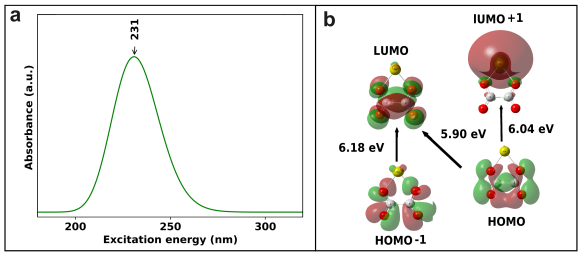

Figure 4: Calculated electronic absorption of calcium oxalate: UV-Vis spectrum (a) and the frontier molecular orbitals significantly contributing to the electronic transitions (b).

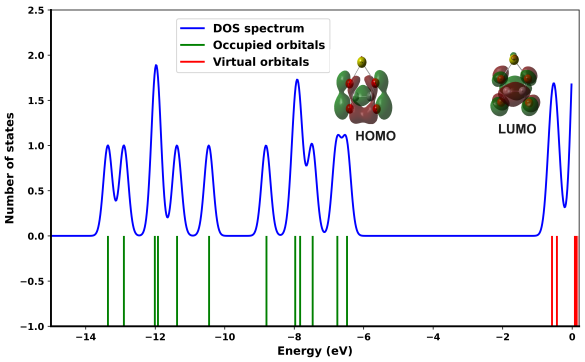

Figure 5: Density of state spectrum along with the occupied and virtual orbitals in calcium oxalate.

Table 1: Calculated electronic properties of calcium oxalate.

Maximum absorption wavelength (nm)	Oscillatory strength	Major contributions	Absorption wavelength of whewellite (nm) [36]
278	0.000	HOMO → LUMO (99%)	288
265	0.000	HOMO-1 → LUMO (99%)	-
231	0.008	HOMO → LUMO+1 (97%)	236

Table 2: Calculated global reactivity descriptors of calcium oxalate.

Ionization potential (I) (eV)	Electron affinity (A) (eV)	Chemical hardness (η) (eV)	Chemical softness (S) (eV)$^{-1}$	Electronic chemical potential (μ) (eV)	Global electrophilicity index (ω) (eV)
6.48	0.58	2.95	0.34	-3.53	2.11

3.2.3 Global reactivity descriptors

The chemical hardness and electrophilicity index of calcium oxalate is obtained to be 2.95 eV and 2.11 eV, respectively (Table 2). These positive values of chemical hardness and electrophilicity index suggest that the compound is suitable for charge transfer processes and can influence the binding energy in protein-ligand interactions [39].

3.2.4 Molecular electrostatic potential and Mulliken atomic charges

Polar regions around the atoms of calcium oxalate are demonstrated with different color codes ranging from -0.316 a.u. to 0.316 a.u. using MEP map. The intense positive potential is observed around the Ca7 and negative potential is found around the O1, O2, O3, and O4 atoms (Figure 6a).

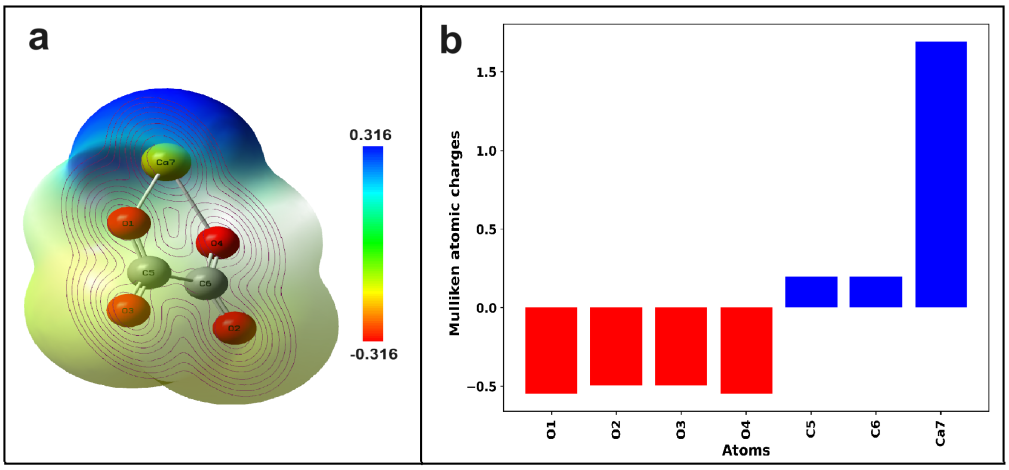

Figure 6: MEP map with contour lines (a) and Mulliken atomic charges contributed by each atom (b) in calcium oxalate molecule.

Further, calcium atom has the maximum positive Mulliken atomic charges and O1 as well as O4 show the maximum negative Mulliken atomic charges (Figure 6b). The variation of charges in oxygen atoms illustrates the induction effect of calcium atom to the bonded oxygen atoms. The MEP map and Mulliken atomic charge distribution show the similar nucleophilic and electrophilic regions in calcium oxalate. The reactive nature of the chemical compound associated with the polar property can be explained using MEP and Mulliken atomic charges [40]. And, the polar nature of calcium oxalate is significant for the bonded and non-bonded interactions with lysozyme protein (Figure 9).

3.3 Interactions of CaC_2O_4 with lysozyme

Lysozyme protein (7xf6.pdb) contains an acetate ion ($C_2H_3O_2$) as a native ligand, which forms non bonded interactions with Ile77, Trp82, Ala126, and Trp127 and hydrogen-bonded (H-bonded) interaction with Asn78 (Figure 8a). All non-glycine residues except Cys134 and Ser54 confine within the most allowed regions of the Ramachandran plot

(Figure 7 and Table 3), indicating that the structure of lysozyme is valid and suitable for the protein-ligand interactions [41, 42].

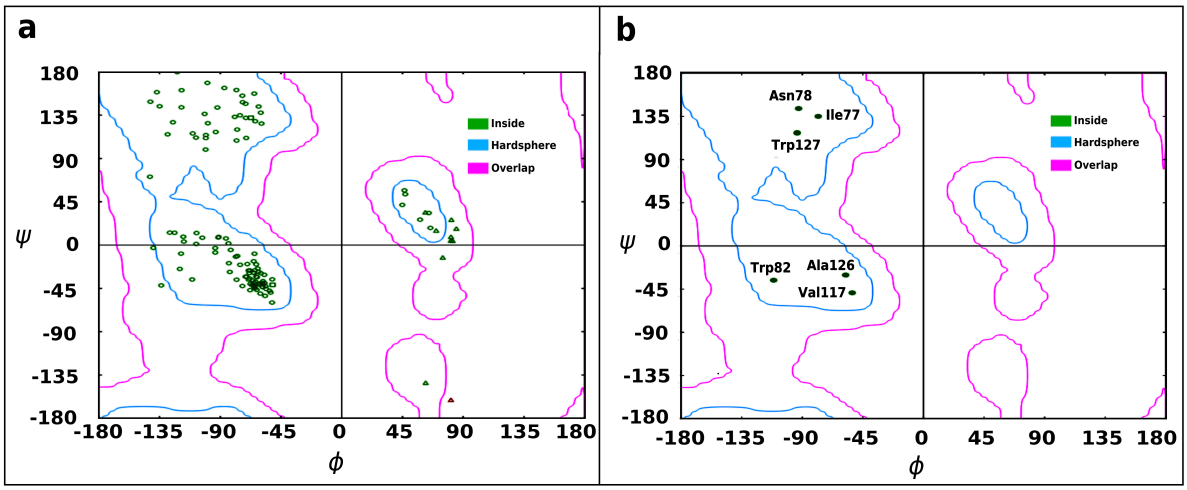

Figure 7: Ramachandran plots: all residues of lysozyme (a) and residues interacting with calcium oxalate (b).

Table 3: Dihedral angle pairs (in degree) of active amino acids of lysozyme interacting with calcium oxalate.

Active amino acids of lysozyme protein	**Dihedral angle (ϕ)**	**Dihedral angle (ψ)**
Ile77	-75.37	134.83
Asn78	-92.15	142.91
Trp82	-110.81	-35.76
Val117	-52.71	-49.32
Ala126	-57.33	-30.91
Trp127	-93.36	117.50

The binding pocket identified using CASTp (Figure 8b) includes active residues Glu53, Asp71, Gln76, Ile77, Asn78, Trp82, Val117, Ala126, Trp127, Val128, and Ala129 with a total binding pocket area 71.823 Å^2 and volume 49.887 Å^3, respectively. This result suggests that the region identified by CASTp closely matches with the location of native ligand, making it suitable for molecular docking between lysozyme and calcium oxalate. The visualizations of the best docked pose of lysozyme-calcium oxalate complex within the binding pocket are shown in Figure 9. The residue Asn78 forms H-bond, while the residues Ile77, Trp82, Val117, Ala126, and Trp127 contribute in hydrophobic interactions with calcium oxalate (Figures 9b,c). These interactions contribute the binding energy of −4.18 kcal/mol (Table 4). This result indicates that the binding affinity of calcium oxalate with lysozyme is slightly higher than that of lactoferrin as shown in our previous work [14]. The present molecular docking analysis suggests that the calcium oxalate, a key component in kidney stones, exhibits a high binding efficacy within the active region of the lysozyme, promoter protein in neprolithiasis. Lysozyme is one of the key proteins found in the matrix of whewellite-type urinary calculi [16]. In *in vivo* conditions, matrix proteins of the calculi can exhibit aggregation-inducing properties, which can enhance the particle size of calcium oxalate type crystals, facilitating crystal growth in urinary tract [43].

The location, size, and type of urinary calculi in a urinary tract significantly influence the treatment modalities. Calculi larger than 7 mm are unlikely to

move spontaneously through urine and typically require surgical intervention. Further, calculi ranging from 1.1 cm to 2.4 cm in size are ideal for breaking using the extracorporeal shockwave lithotripsy (ESWL) and greater than 2 cm are recommended for percutaneous nephrolithotomy (PCNL) techniques [44–46]. Among different calculi, weddellite types are relatively easy to break. In contrast, whewellite, infected struvite, and cystine offer the highest resistance to the ESWL. Generally, Ureteroscopy (URS) is better option for treatment of cystine type calculi [44, 46].

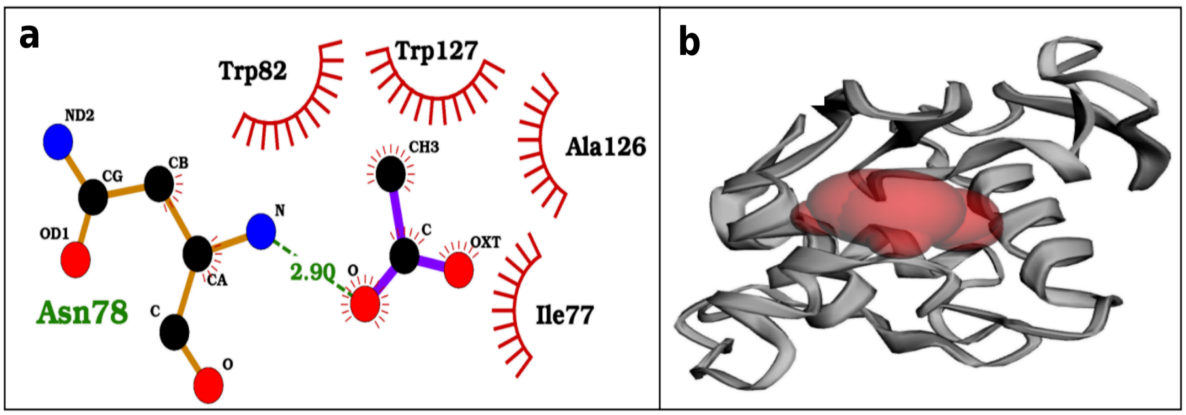

Figure 8: Interactions of native ligand, acetate ion ($C_2H_3O_2$), with lysozyme (7xf6.pdb) are represented by spoked arcs for nonbonded residues, green-dotted line for hydrogen bond, and written in green color for hydrogen-bonded residue using LigPlot+ v.2.2 (a). The location of the binding pocket highlighted in red within the lysozyme represented using ribbon like structure generated by CASTp (b).

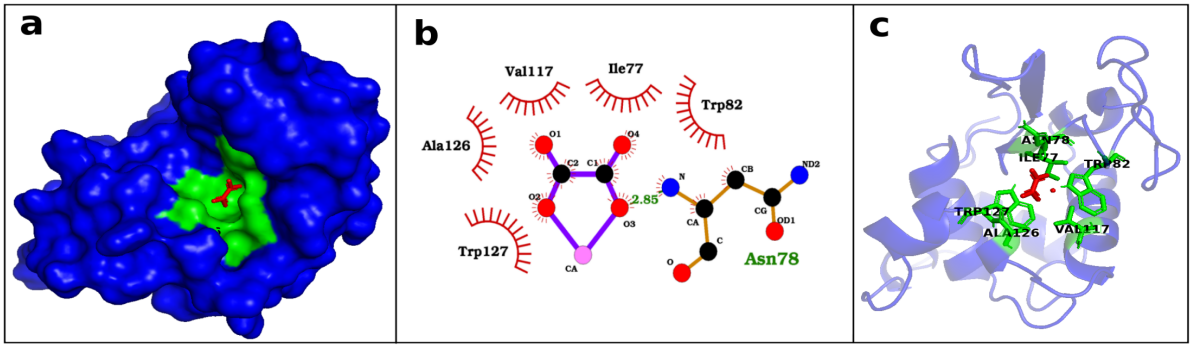

Figure 9: Calcium oxalate (red) within the binding pocket of lysozyme (green for interacting and blue for non interacting residues) visualized using PyMOL (a,b). Interactions of calcium oxalate with lysozyme are illustrated with nonbonded residues shown as spoked arcs, hydrogen-bonded residue indicated in green color, generated using LigPlot+ v.2.2 (c).

Table 4: Molecular docking results of calcium oxalate with lysozyme at temperature 298.15 K.

Energy components	**Energy (kcal/mol)**
van der Waals, hydrogen bond, and disolvation energy	-4.16
Electrostatic Energy	-0.02
Total binding energy	-4.18

4 Conclusion

This work is focused on the characterization of kidney stones and the study of nephrolithiasis phenomena using FTIR, DFT, and molecular docking approaches. The characterization of kidney stones using spectroscopic techniques reveals that the majority are composed of calcium oxalate monohydrate. The quantum mechanical properties suggest that calcium oxalate can interact through bonded and non-bonded interactions with proteins. The molecular docking analysis of calcium oxalate within the binding regions of lysozyme shows effective binding interactions. Hence, lysozyme can play potential role for the development of calcium oxalate type nephrolithiasis. In summary, this research finds the distribution of the types of kidney stones and contributes to understand the phenomena of calcium oxalate type nephrolithiasis, which remains still unclear and is one of the most challenging global problems for the scientific community. Further, characterization of kidney stones from different regions using a large sample size and the study of nephrolithiasis using different promoter and inhibitor macromolecules from both experimental and *in silico* approaches are still necessary for a detailed understanding of this global challenge.

Competing interests

The authors declare that there is no conflict of interest.

Ethics approval and consent to participate

This study was conducted with the approval of the institutional review committee of the Institute of Medicine, Tribhuvan University Teaching Hospital, Maharajgunj, Kathmandu, Nepal with an approval number of 117 (6-11) E2 079/080. Informed consent was received from participants or their parents or legal guardians.

Data availability

The data supporting the findings of this study are available within the article.

Authors' contributions

A Acharya: Conceived and designed the experiments, performed data analysis, prepared the figures, and wrote the manuscript
M Khanal: Data analysis, manuscript writing
R Maharjan: Technical support, critical feed back and revised the manuscript
K Gyawali: Critical feed back and revised the manuscript
K Khanal: Critical feed back and revised the manuscript
MB Kshetri: Critical feed back and revised the manuscript
BR Luitel: Critical feedback, data analysis, and revised the manuscript
R Adhikari: Critical feedback, data analysis, and revised the manuscript
DD Mulmi: Critical feedback and revised the manuscript
TR Lamichhane: Technical support, critical feedback, data analysis, and revised the manuscript
HP Lamichhane: Critical feedback, data analysis and revised the manuscript

Acknowledgment

We would like to express our gratitude to Prof. Dr. Rajendra Parajuli and Asst. Prof. Pitamber Shrestha, Amrit campus, T. U., for their invaluable support in providing access to Gaussian 16W software. Additionally, we extend our sincere thanks to Dr. Rabindra Tamang, Dr. Purushottam Parajuli, Dr. Anjit Phuyal, and Dr. Milan Gyawali for their unwavering assistance in the collection of kidney stones. Lastly, we are deeply grateful to Mr. Bidit Lamsal and Mr. Yub Narayan Thapa for their support in generating the FTIR spectra and Dr. Jhashanath Adhikari Subin for the suggestion in molecular docking analysis. Without the collective efforts of these remarkable individuals, this project would not have been possible.
This research is partially supported by the Research Endowment Fund (REF) at Tribhuvan University, Rector's Office, Research Directorate, Kathmandu, Nepal.

References

[1] W. Shang et al. History of kidney stones and risk of chronic kidney disease: a meta-analysis. *Peer J*, 5:e2907, 2017. https://doi.org/10.7717/peerj.2907

[2] H.L. Norbert et al. Acute kidney injury: an increasing global concern. *The Lancet*, 382:170–179, 2013. https://doi.org/10.1016/S0140-6736(13)60647-9

[3] N. Aiumtrakul et al. Global trends in kidney stone awareness: A time series analysis from 2004–2023. *Clin. Pract.*, 14e:915–927e, 2024. https://doi.org/10.3390/clinpract14030072

[4] S. Igor et al. Epidemiology of stone disease across the world. *World J. Urol.*, 35:1301–1320, 2017. https://doi.org/10.1007/s00345-017-2008-6

[5] Y. Liu et al. Epidemiology of urolithiasis in asia. *Asian J Urol.*, 5:205–214, 2018. https://doi.org/10.1016/j.ajur.2018.08.007

[6] H.N. Joshi et al. Epidemiology of urolithiasis in asia. *Kathmandu Univ. Med. J.*, 18:90–93, 2020.

[7] S. Pokhrel and S. Acharya. Role of computed tomography urography in evaluation of patients with obstructive uropathy. *J. KIST Med. Col.*, 5:48–52, 2023.

[8] S. Koirala. Significance of analysing chemical composition of renal stones. *J. Pathol. Nepal.*, 4:560–564, 2014. https://doi.org/10.3126/jpn.v4i7.10314

[9] B. Bhandari et al. Infrared spectroscopic analysis of chemical composition of urolithiasis among serving nepalese soldiers- an institutional study. *Med. J. Shree Birendra Hosp.*, 21:6–10, 2022. https://doi.org/10.3126/mjsbh.v21i2.42802

[10] K. Stamatelou and D.S. Goldfarb. Epidemiology of kidney stones. *Healthcare*, 11:424, 2023. https://doi.org/10.3390/healthcare11030424

[11] S. Nicolau and A.J. Matzger. An evaluation of resolution, accuracy, and precision in ft-ir spectroscopy. *Spectrochim. Acta - Part A Mol. Biomol. Spectrosc.*, 319:124545, 2024. https://doi.org/10.1016/j.saa.2024.124545

[12] V. Asyana et al. Analysis of urinary stone based on a spectrum absorption ftir-atr. *J. Phys.: Conf. Ser.*, 694:012051, 2016. https://doi.org/10.1088/1742-6596/694/1/012051

[13] J. Tonannavar et al. Identification of mineral compositions in some renal calculi by ft raman and ir spectral analysis. *Spectrochim. Acta - Part A Mol. Biomol. Spectrosc.*, 154:20–26, 2016. https://doi.org/10.1016/j.saa.2015.10.003

[14] A. Acharya et al. Quantum chemical calculations on calcium oxalate and dolichin a and their binding efficacy to lactoferrin: An *in silico* study using dft, molecular docking, and molecular dynamics simulations. *AIMS Biophys.*, 11:142–165, 2024. https://doi.org/10.3934/biophy.2024010

[15] M. Khanal et al. Identification of potent inhibitors of hdac2 from herbal products for the treatment of colon cancer: Molecular docking, molecular dynamics simulation, mm/gbsa calculations, dft studies, and pharmacokinetic analysis. *PloS one*, 19:e0307501, 2024. http://dx.doi.org/10.1371/journal.pone.0307501

[16] S. Farmanesh et al. Natural promoters of calcium oxalate monohydrate crystallization. *J. Am. Chem. Soc.*, 136:12648–12657, 2014. https://doi.org/10.1021/ja505402r

[17] X. Meng et al. Molecular docking: A powerful approach for structure-based drug discovery. *Curr. Comput. Aided Drug Des.*, 7:146–157, 2011. https://doi.org/10.2174/157340911795677602

[18] B. Chattaraj et al. Inhibitory activity of enhydra fluctuans lour. on calcium oxalate crystallisation through *in silico* and *in vitro* studies. *Front. Pharmacol.*, 13:1102465, 2023. https://doi.org/10.3389/fphar.2022.982419

[19] S. Kim et al. Pubchem 2023 update. *Nucleic Acids Res.*, 51:D1373–D1380, 2023. https://doi.org/10.1093/nar/gkac956

[20] M. J. Frisch et al. *Gaussian 16 Revision C.01*. Gaussian Inc. Wallingford CT. https://gaussian.com/gaussian16/

[21] R. G. Pearson. Absolute electronegativity and hardness: application to inorganic chemistry. *Inorg. Chem.*, 27:734–740, 1988. https://doi.org/10.1021/ic00277a030

[22] P. Geerlings et al. Conceptual density functional theory. *Chem. Rev.*, 103:1793–1874, 2003. https://doi.org/10.1021/cr990029p

[23] J. Padmanabhan et al. Electrophilicity-based charge transfer descriptor. *J. Phys. Chem. A*, 111:1358–1361, 2007. https://doi.org/10.1021/jp0649549

[24] R. Dennington et al. *GaussView Version 6*. Semichem Inc. Shawnee Mission KS. https://gaussian.com/gaussview6/

[25] N. M. O'boyle et al. Cclib: a library for package-independent computational chemistry algorithms. *J. Comput. Chem.*, 29:839–845, 2008. https://doi.org/10.1002/jcc.20823

[26] K. H. Nam. Crystal structure of human lysozyme complexed with n-acetyl--d-glucosamine. *Appl. Sci.*, 12:4363, 2022. https://doi.org/10.3390/app12094363

[27] Dassault Systemes; San Diego, CA, USA Version v21.1.0.20298. *Biovia Discovery Studio Visualizer*. https://www.3ds.com/products/biovia/discovery-studio

[28] B. Ye et al. Castpfold: Computed atlas of surface topography of the universe of protein folds. *Nucleic Acids Res.*, 52:W194–W199, 2024. https://doi.org/10.1093/nar/gkae415

[29] G. M. Morris et al. Autodock4 and autodocktools4: Automated docking with selective receptor flexibility. *J. Comput. Chem.*, 30:2785–2791, 2009. https://doi.org/10.1002/jcc.21256

[30] S. Forli et al. Computational protein-ligand docking and virtual drug screening with the autodock suite. *Nat Protoc.*, 11:905–919, 2016. https://doi.org/10.1038/nprot.2016.051

[31] S. Cosconati et al. Virtual screening with autodock: theory and practice. *Expert Opin. Drug Discovery.*, 5:597–607, 2010. https://doi.org/10.1517/17460441.2010.484460

[32] R. Maharjan et al. Artemisinin derivatives as potential drug candidates against mycobacterium tuberculosis: insights from molecular docking, md simulations, pca, mm/gbsa and admet analysis. *Mol. Simul.*, 50:717–728, 2024. https://doi.org/10.1080/08927022.2024.2346525

[33] *Schrödinger, LLC The PyMOL Molecular Graphics System, Version 1.8*, 2015.

[34] R. A. Laskowski and M. B. Swindells. Ligplot+: multiple ligand-protein interaction diagrams for drug discovery. *J. Chem. Inf. Model.*, 51:2778–2786, 2011. https://doi.org/10.1021/ci200227u

[35] E. J. Lien et al. Use of dipole moment as a parameter in drug-receptor interaction and quantitative structure-activity relationship studies. *J. Pharm. Sci.*, 71:641–655, 1982. https://doi.org/10.1002/jps.2600710611

[36] A. Ahmad et al. Hybrid crystal stones physicochemical and morphological characterization: A spectroscopic study analysis. *Hybrid Advances*, 6:100259, 2024. https://doi.org/10.1016/j.hybadv.2024.100259

[37] R. Mishra et al. Quantum chemical and experimental studies on the structure and vibrational spectra of an alkaloid-corlumine. *Spectrochim. Acta Part A Mol. Biomol. Spectrosc.*, 118:470–480, 2014. https://doi.org/10.1016/j.saa.2013.09.015

[38] R. Fouad and O. M. Adly. Novel cu2+ and zn2+ nanocomplexes drug based on hydrazone ligand bearings chromone and triazine moieties: structural, spectral, dft, molecular docking and cytotoxic studies. *J. Mol. Struct.*, 1225:129158, 2021. https://doi.org/10.1016/j.molstruc.2020.129158

[39] R.G. Parr, L. von Szentpály, and S. Liu. Electrophilicity index. *J. Am. Chem. Soc.*, 121:1922–1924, 1999. https://doi.org/10.1021/ja983494x

[40] M. Karakus Z. Demircioğlu and E. Sancakli. Theoretical analysis (nbo, npa, mulliken population method) and molecular orbital studies (hardness, chemical potential, electrophilicity and fukui function analysis) of (e)-2-((4-hydroxy-2-methylphenylimino) methyl)-3-methoxyphenol. *J. Mol. Struct.*, 1091:183–195, 2015. https://doi.org/10.1016/j.molstruc.2015.02.076

[41] G.N. Ramachandran, C. Ramakrishnan, and V. Sasisekharan. Stereochemistry of polypeptide chain configurations. *J. Mol. Biol.*, 7:95–99, 1963. https://doi.org/10.1016/S0022-2836(63)80023-6

[42] T.R. Lamichhane and M.P. Ghimire. Evaluation of sars-cov-2 main protease and inhibitor interactions using dihedral angle distributions and radial distribution function. *Heliyon*, 7:e08220, 2021. https://doi.org/10.1016/j.heliyon.2021.e08220

[43] K.R. Saeed and H.L. Raymond. Role of organic matrix in urinary stone formation: An ultrastructural study of crystal matrix interface of calcium oxalate monohydrate stones. *J. Urol.*, 150:239–245, 1993. https://doi.org/10.1016/S0022-5347(17)35454-X

[44] J. Dzelaludin and K. Dzelaludin. Evaluation of extracorporeal shock wave lithotripsy (eswl): Efficacy in treatment of urinary system stones. *Acta Inform. Med.*, 22:309–314, 2014. https://doi.org/10.5455%2Faim.2014.22.309-314

[45] K. Dmitriy and P. Aleksandr. Only size matters in stone patients: Computed tomography controlled stone-free rates after mini-percutaneous nephrolithotomy. *Urol. Int.*, 103:166–171, 2019. https://doi.org/10.1159/000497442

[46] G.J. David and P.S. Margaret. The contemporary management of renal and ureteric calculi. *BJU Int.*, 98:1283–1288, 2006. https://doi.org/10.1111/j.1464-410X.2006.06514.x